Microseismicity illuminates open fractures in the shallow crust

Stella I. Pytharouli,[1] Rebecca J. Lunn,[1] Zoe K. Shipton,[1,2] James D. Kirkpatrick,[2,3] and Aderson F. do Nascimento[4]

Received 18 October 2010; revised 7 December 2010; accepted 20 December 2010; published 29 January 2011.

[1] Successful delivery of geological carbon storage and/or radioactive waste disposal relies on the ability to predict the transport of waste stored/disposed of at depth, over 10^3 to 10^6 years. Field evidence shows that faults and fractures can act as focused pathways for contaminant migration. Hence, transport predictions require detailed characterization of fracture location, orientation and hydraulic properties. We show that microseismic monitoring can delineate the three-dimensional structure and hydraulic characteristics of flowing fractures at 2 to 3 km depth. Individual fracture planes are validated by independently derived composite focal mechanisms. Local field observations confirm the presence of open fractures with lengths and orientations matching the seismically-derived fracture planes. The temporal evolution of seismicity within individual fractures allows us to estimate depth-averaged transmissivity and in-plane fluid velocity distributions. Our results demonstrate the potential of microseismic monitoring to characterize flowing fractures, for non-invasive site investigation at CO_2 and radioactive waste storage/disposal sites. **Citation:** Pytharouli, S. I., R. J. Lunn, Z. K. Shipton, J. D. Kirkpatrick, and A. F. do Nascimento (2011), Microseismicity illuminates open fractures in the shallow crust, *Geophys. Res. Lett.*, *38*, L02402, doi:10.1029/2010GL045875.

1. Introduction and Geological Setting

[2] Geological carbon storage and radioactive waste disposal require proof of robust geosphere containment over 10^3 to 10^6 years. Such containment relies on the integrity of the surrounding rocks to inhibit upward migration of liquids and gases from a storage site/repository. Field evidence shows that fractures have the potential to act as focused pathways for rapid fluid movement to the Earth's surface and that the hydraulic properties of fractured rock may vary substantially over the timescales required for containment [*Eichhubl and Boles*, 2000; *Claesson et al.*, 2007]. Here we show that detailed microseismic monitoring can be used to image, and hydraulically characterize, the three-dimensional structure of open fractures up to 2.5 km depth.

[3] It is common to fit a single surface to a planar cloud of earthquakes to define the location and orientation of the fault that is hosting the earthquakes [*Carena et al.*, 2002; *Geiser and Seeber*, 2008; *Julian et al.*, 2010; *El Hariri et al.*, 2010]. For a fluid-driven aftershock sequence, temporal migration within such a cloud can be used to estimate a value for fault permeability [*Miller et al.*, 2004]. A recent study, with exceptionally well-located earthquakes, has shown that for earthquakes induced by magma intrusion, microseismic clouds that appear to be localized along the intruding margin can actually be resolved onto a number of individual fracture surfaces [*Carmona et al.*, 2010]. This suggests that such aftershocks are delineating structural heterogeneities within a wider microseismic zone and that they could be used to explore the heterogeneous nature of fracture hydraulics.

[4] For geological storage of CO_2 and radioactive waste disposal, detailed characterization of faults and fractures is required for probabilistic simulations of long-term contaminant migration. For instance, it is critical to predict dilution and the distribution of arrival times of radioisotopes at the Earth's surface when preparing a safety case for geological disposal of radioactive waste. For geothermal energy, researchers have used induced microseismicity to derive an anisotropic bulk permeability tensor for the host rock surrounding an injection borehole [*Fischer et al.*, 2008]. No comparable methodology exists, however, for locating individual fracture surfaces within a large rock volume (several km^2) and for estimating their size, orientation and hydraulic properties. If induced microseismicity could be used to provide such data, it would be an invaluable tool. Microseismicity is a well-known consequence of CO_2 injection [*Zhou et al.*, 2010], and in radioactive waste disposal, long-term borehole injection tests are common. Hence in both cases, detailed microseismic (or nanoseismic [*Wust-Bloch*, 2010]) monitoring could be deployed over long time-scales.

[5] We use reservoir-induced seismicity beneath Açu Reservoir in North East Brazil to characterize fractures at depth. The reservoir is situated on Archean gneisses and Neoproterozoic granites [*Almeida et al.*, 2000] (Figure 1). The microseismic events, with magnitudes up to 2.1, are caused by groundwater pressure variations (less than 0.5 kPa [*do Nascimento et al.*, 2005]) at depth due to flow induced by seasonal fluctuations in the surface reservoir level [*Ferreira et al.*, 1995] (auxiliary material).[1] Each year, a time lag of approximately 4 months between peak reservoir level and peak seismic activity is observed. Microseismic events recorded from 1994–1997 are concentrated within a 2 km long, 230 to 400 m wide zone. The plane that best fits the cloud of microseismic data is oriented 043/88SE.

[6] The zone of seismicity correlates with the position of one of three previously un-mapped, major brittle faults oriented sub-parallel to the regional foliation (Figure 1). The

[1]Department of Civil Engineering, University of Strathclyde, Glasgow, UK.
[2]Department of Geographical and Earth Sciences, University of Glasgow, Glasgow, UK.
[3]Now at Earth and Marine Sciences Department, University of California, Santa Cruz, California, USA.
[4]Departamento de Geofísica, Universidade Federal do Rio Grande do Norte, Natal, Brazil.

0094-8276/11/2010GL045875

[1]Auxiliary material data sets are available at ftp://ftp.agu.org/apend/gl/2010GL045875. Other auxiliary material files are in the HTML.

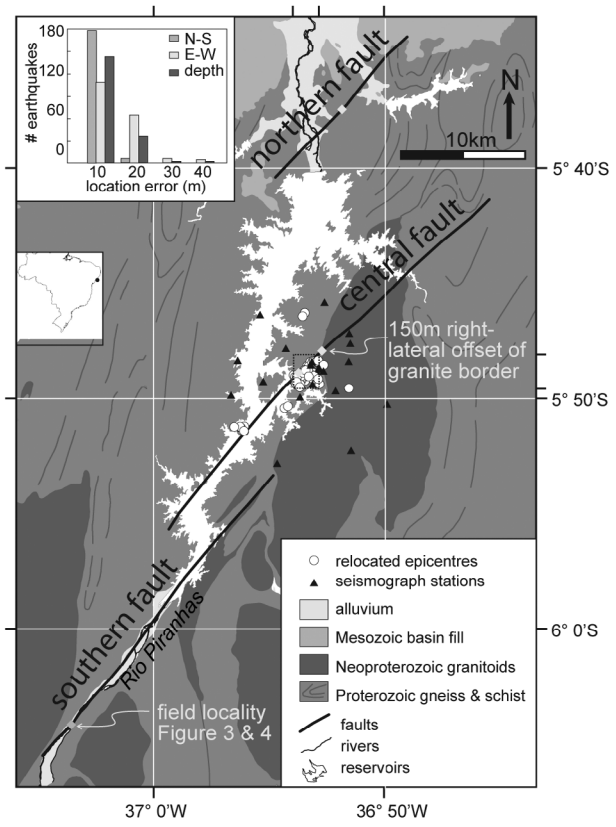

Figure 1. Geologic map of the Açu reservoir area. Solid black lines are faults defined by air photo and Landsat satellite lineaments that have been ground truthed at four field sites (gray diamonds). White circles are the 185 relocated earthquakes, black triangles are the positions of the seismic stations. The black dotted box shows the location of Figure 2. The estimated errors of the relocated hypocenters are also in the inset. Existence of these faults was previously inferred from geomagnetic anomalies [*Oliveira*, 2008].

central fault offsets a Neoproterozoic granite boundary right-laterally by 150 m (Figure 1). Slip vector data and mesoscopic fault geometries along the northern and southern faults indicate that the most recent activity on these faults was dextral strike-slip. The microseismic events are adjacent to the mapped trace of the central fault and their best-fit plane strikes within 2° of the central fault trace. Hence the earthquake events are clearly associated with this fault.

2. Seismicity Data

[7] From 1994–1997 a dense monitoring network of 8 seismometers was deployed throughout 15 locations (Figure 1). A duration magnitude scale (m_D), derived for regional microearthquakes in Brazil was used [*Blum and Assumpção*, 1990]. The detection threshold of the stations was low (a 0.2 m_D event could be detected at 2 km slant distance) and they were periodically relocated to achieve the best coverage of the epicentral area [*do Nascimento et al.*, 2004]. A time delay between the maximum water level and the maximum number of earthquakes supports a triggering mechanism of pressure diffusion from the reservoir [*Talwani and Acree*, 1985; *Simpson et al.*, 1988]. Events are not in the form of a classic aftershock sequence since maximum magnitudes occur during the whole earthquake sequence and the number of earthquakes does not decrease with time (auxiliary material). Similar event sequences are termed "swarm-like" and have been observed at other locations where seismicity is pressure-induced [*Hainzl and Fischer*, 2002; *Kurz et al.*, 2004].

[8] A total of 279 microseismic events were detected, which have been previously accurately located [*El Hariri et al.*, 2010]. To further reduce the location errors, we reapplied the waveform cross-correlation technique [*Rowe et al.*, 2002], introduced a linear function to correct for time drifting on the seismometer clocks, and re-picked the P and S-wave arrival times. Using only earthquakes that were well-recorded by 5 or more stations we relocated 185 events (Figure 1). The majority (109) of the relocated hypocenters have location errors ≤10 m in all three directions, 65 have errors ≤20 m and only 11 have errors between 20 m and 40 m (Figure 1, inset).

[9] Cross-correlation of the waveforms delineated 47 clusters of between 2 and 9 events with highly similar waveforms (defined by a correlation coefficient >0.8). Even the codas of these traces were almost identical (Figure 2a) indicating that the seismic waves followed almost identical paths from the source to the station. Previous researchers have only reported similarly near-identical signals from downhole seismometer data [*Abercrombie*, 1995] for events that are a few meters from the monitoring borehole. The striking waveform similarity implies that clustered events are highly likely to have occurred on the same geological structure [*Geller and Mueller*, 1980; *Poupinet et al.*, 1984].

[10] We test the hypothesis that each cluster of earthquakes occurs on a single structure by fitting a plane to each individual cluster and examining the residuals. Examining residuals requires at least 4 events in a cluster. Of the 47 clusters, eight consisted of over four events (c1 to c8, Figure 2b). For these 8 clusters the direction cosines of the best-fit planes were calculated using singular value decomposition. Three of the clusters (c3, c5 and c7) are best fit by 2 pairs of parallel planes, 41, 124 and 31 m apart respectively (each parallel plane is defined by at least three earthquakes). This results in a total of eleven planes. For each plane the residuals, i.e. the perpendicular distances of the hypocenters from the fitted plane, were less than the earthquake location errors (in the case of cluster 7, one of the parallel planes had no residuals as the plane was defined by 3 points only).

[11] The fitted planes were independently validated by deriving composite focal mechanisms for each cluster (Figure 2c). For four clusters the fitted planes were entirely consistent with the focal mechanisms. For four clusters an adjustment of less than 20° was required to the strike and/or dip of the nodal planes (auxiliary material). The perpendicular distance of the hypocenters to the planes is less than 20 m for 32 earthquakes, 20 to 40 m for 7 earthquakes, and 40 to 70 m for 3 earthquakes. These residuals are less than previously published source dimensions for earthquakes of this magnitude [*Tomic et al.*, 2009] and, with the exception of two earthquakes, are within the uncertainties of the earthquake locations.

3. Field Data

[12] To confirm the presence of open fractures with orientations consistent with those of the microseismic cluster

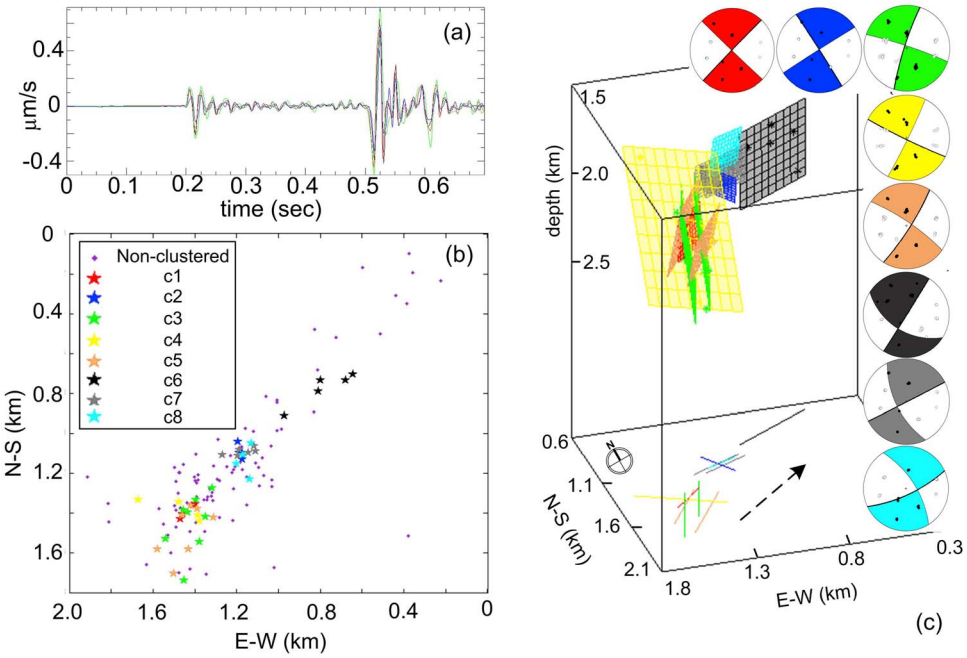

Figure 2. Seismic data analysis. (a) Stacked waveforms for cluster c1. (b) Plan view of relocated epicenters in the highlighted area in Figure 1. At this scale the symbols are bigger than the errors in the locations of the earthquakes. (c) Best-fit planes to clusters c1 to c8. The trace of each plane at a depth of 1.9 km is projected on the base. The planes are sub-parallel to a zone trending ~043° (dashed arrow). Composite focal mechanisms of each cluster are consistent with modern-day E–W compressive stress [*Ferreira et al.*, 1995].

planes, we mapped an exceptionally well-exposed site on the southern fault (Figure 3). Open fracture zones initiate at the boundary of a 2 to 5 m-wide fault core composed of well-cemented breccias and cataclasites, they extend across the fault damage zone, containing veins of epidote, quartz and chlorite (typical mid-crustal minerals formed at temperatures of 200–250°C), and they continue into the host rock. No fracture zones terminated before being covered by alluvial sediments and the longest an individual fracture could be traced was 100 m.

[13] Our field observations suggest that rather than modern-day flow being focused within a fault damage zone that formed during fault growth [*Evans et al.*, 1997], flow is occurring within a zone of younger open fractures. The open fractures probably initiated due to the mechanical contrast between the core and the surrounding rock during uplift and exhumation of the fault zone. The field observations are consistent with the microseismicity data; earthquakes are not occurring on a single surface defined by a best-fit plane to the event locations, instead, they are hosted by multiple planes in a 230 to 400 m wide zone (Figure 2). The orientation of the zone of microseismicity confirms its relationship to the central fault, however, its width indicates it is not a conventional fault damage zone since previous studies predict this to be between 0.001 to 0.1 of fault offset [*Shipton et al.*, 2006]. Consequently, at this location conventional models of fault damage zones controlling flow in crystalline rocks would severely underestimate the width of the zone of flowing features.

4. Flow and Permeability

[14] To predict flow within the fractures defined by the microseismic data, a statistical distribution of fracture permeabilities is required. Following the methodology of *Talwani et al.* [2007] we estimate, for each plane in Figure 2, a depth-averaged permeability value based on the time between peak reservoir and the onset of seismicity, and the location of the first event within each cluster (Figure 4a, grey, and auxiliary material). Our field observations of the open fractures show them to be well-connected along strike, with no observable fill (Figure 4b). Hence, we suggest that subsequent events within any one plane are triggered by a pressure pulse generated by the first in-plane event. Using the time and distance of subsequent events from the first in-plane event, we then estimate a distribution for within-plane permeability at micro-seismic depths of 1.5–2.5 km (Figure 4a, black, and auxiliary material). Our results show that the peak in within-plane permeability is two orders of magnitude smaller than that of the depth-averaged permeability, which is consistent with increasing normal stress over depth. Furthermore, the within-plane permeability distribution ranges from 10^{-15} to 10^{-20} m^2, (Figure 4a, black), whereas the average permeability (Figure 4a, grey) only varies from 10^{-15} to 10^{-17} m^2, which is consistent with the latter being depth-averaged. Hence, the within-plane permeability distribution is describing hydraulic heterogeneity within the fractures at 1.5–2.5 km depth.

5. Conclusions

[15] This research shows that exceptionally well-located microseismic data can be used to identify the locations, orientations and transmissivities of open fractures at 1.5 to 2.5 km depth. No other geophysical data can be used to identify individual large-scale open fractures within such a substantial rock volume, or their hydraulic properties. Similar

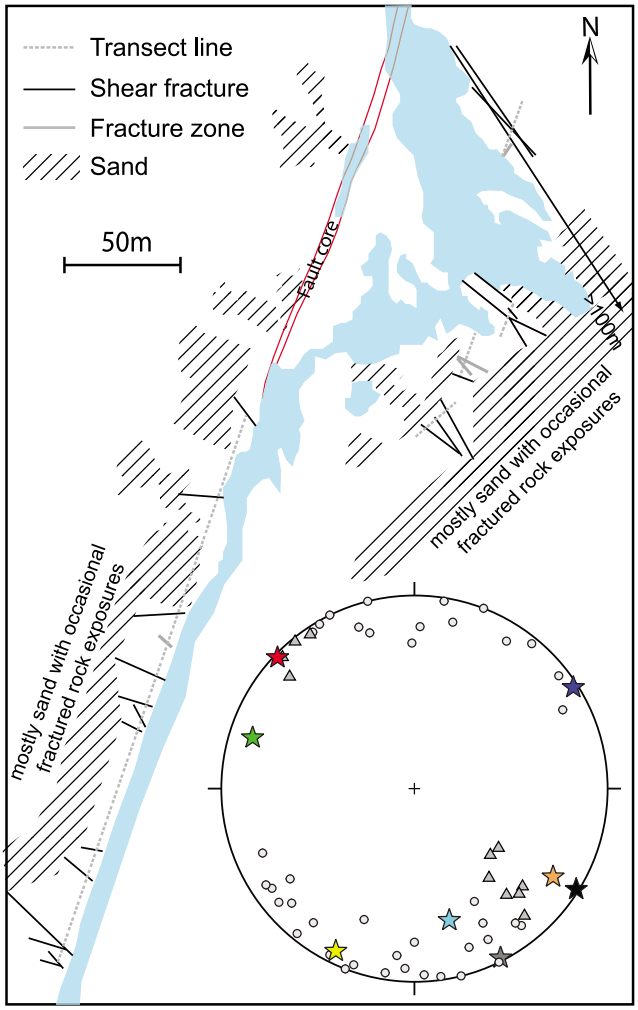

Figure 3. Field map (location shown on Figure 1) based on transect data. Fracture zones are defined by interconnected, sub-parallel and conjugate fractures clustered into planar, brittle shear zones up to 1 m wide. Inset: Stereonet showing orientation of the mapped fractures and fracture zones (circles) compared to the poles to the fitted earthquake cluster planes (stars colored to match planes in Figure 2) and the exposed fault core (triangles).

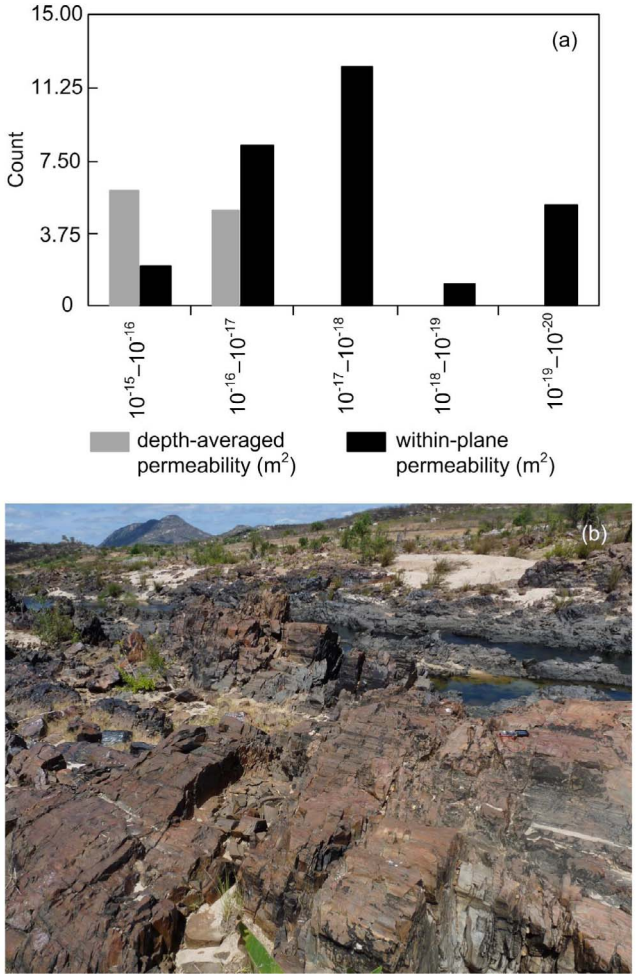

Figure 4. (a) Histogram of depth-averaged permeability (black) and within-plane permeability (gray) for the fitted planes. (b) Photograph showing the open, unfilled fractures/fracture zones. The fractures/fracture zones support the hypothesis of long, transmissive, open features, well-connected along strike, within which pressure waves propagate to trigger the initial and subsequent microseismic events.

long-term high-quality baseline microseismic monitoring data should be collected at CO_2/radioactive waste disposal sites. This may require the installation of multiple down-hole seismometers to achieve the required earthquake location accuracy and long-term monitoring to capture multiple events on individual planes. The resulting microseismic data will provide a new capability to image large-scale flowing features, the locations and hydraulic characteristics of which can be used to inform risk assessment models and to plan effective monitoring strategies.

[16] **Acknowledgments.** We thank W. Sloan, D. Healey, J. S. Caine, E. B. Brodsky, and U. Balthazar for discussions and reading of the manuscript. We thank R. Abercrombie for useful suggestions during the relocation process and A. Soden for assistance with Figure 3. This work was funded by UK Natural Environment Research Council grant NE/E004210/1 to R.J.L. and NE/E005365/1 to Z.K.S. A.F.dN. thanks CNPq for grants 303706/2008-2 and 483349/2007-0. This paper benefited from the reviews of P. Younger and J. Fairley.

References

Abercrombie, R. E. (1995), Earthquake locations using single-station deep borehole recordings: Implications for microseismicity on the San Andreas Fault in southern California, *J. Geophys. Res.*, *100*(B12), 24,003–24,014, doi:10.1029/95JB02396.

Almeida, F. F. M., B. B. Brito Neves, and C. D. R. Carneiro (2000), The origin and evolution of the South American Platform, *Earth Sci. Rev.*, *50*, 77–111, doi:10.1016/S0012-8252(99)00072-0.

Blum, M. L., and M. Assumpção (1990), Estimativa do parâmetro b dos sismos de Palhano, CE, de outubro de 1988 (in Portuguese), in *XXXVI Congresso Brasileiro de Geologia, Anais*, vol. 5, pp. 2160–2163, Soc. Bras. de Geol., Natal, Brazil.

Carena, S., J. Suppe, and H. Kao (2002), The active detachment of Taiwan illuminated by small earthquakes and its control on first-order topography, *Geology*, *30*, 935–938, doi:10.1130/0091-7613(2002)030<0935:ADOTIB>2.0.CO;2.

Carmona, E., J. Almendros, J. A. Peña, and J. M. Ibáñez (2010), Characterization of fracture systems using precise array locations of earthquake multiplets: An example at Deception Island volcano, Antarctica, *J. Geophys. Res.*, *115*, B06309, doi:10.1029/2009JB006865.

Claesson, L., C. Skelton, C. Graham, and C. M. Morth (2007), The timescale and mechanisms of fault sealing and water-rock interaction after an earthquake, *Geofluids*, *7*, 427–440, doi:10.1111/j.1468-8123.2007.00197.x.

do Nascimento, A., P. A. Cowie, R. J. Lunn, and R. G. Pearce (2004), Spatio-temporal evolution of induced seismicity at Açu reservoir, NE Brazil, *Geophys. J. Int.*, *158*, 1041–1052, doi:10.1111/j.1365-246X.2004.02351.x.

do Nascimento, A. F., R. J. Lunn, and P. A. Cowie (2005), Modeling the heterogeneous hydraulic properties of faults using constraints from reservoir-induced seismicity, *J. Geophys. Res.*, *110*, B09201, doi:10.1029/2004JB003398.

Eichhubl, P., and J. R. Boles (2000), Rates of fluid flow in fault systems: Evidence for episodic rapid fluid flow in the Miocene Montery formation, coastal California, *Am. J. Sci.*, *300*, 571–600, doi:10.2475/ajs.300.7.571.

El Hariri, M., R. E. Abercrombie, C. A. Rowe, and A. F. do Nascimento (2010), The role of fluids in triggering earthquakes: Observations from reservoir induced seismicity in Brazil, *Geophys. J. Int.*, *181*, 1566–1574.

Evans, J. P., C. B. Forster, and J. V. Goddard (1997), Permeability of fault-related rocks, and implications for hydraulic structure of fault zones, *J. Struct. Geol.*, *19*(11), 1393–1404, doi:10.1016/S0191-8141(97)00057-6.

Ferreira, J. M., R. T. De Oliveira, M. Assumpcão, J. A. M. Moreira, R. G. Pearce, and M. K. Takeya (1995), Correlation of seismicity and water level in the Açu reservoir: An example from northeastern Brazil, *Bull. Seismol. Soc. Am.*, *85*, 1483–1489.

Fischer, T., S. Hainzl, L. Eisner, S. A. Shapiro, and J. Le Calvez (2008), Microseismic signatures of hydraulic fracture growth in sediment formations: Observations and modelling, *J. Geophys. Res.*, *113*, B02307, doi:10.1029/2007JB005070.

Geiser, P. A., and L. Seeber (2008), Three-dimensional seismo-tectonic imaging: An example from the Southern California Transverse Ranges, *J. Struct. Geol.*, *30*(7), 929–945, doi:10.1016/j.jsg.2008.02.010.

Geller, R. J., and C. S. Mueller (1980), Four similar earthquakes in central California, *Geophys. Res. Lett.*, *7*(10), 821–824, doi:10.1029/GL007i010p00821.

Hainzl, S., and T. Fischer (2002), Indications for a successively triggered rupture growth underlying the 2000 earthquake swarm in Vogtland/NW Bohemia, *J. Geophys. Res.*, *107*(B12), 2338, doi:10.1029/2002JB001865.

Julian, B. R., G. R. Foulger, F. C. Monastero, and S. Bjornstad (2010), Imaging hydraulic fractures in a geothermal reservoir, *Geophys. Res. Lett.*, *37*, L07305, doi:10.1029/2009GL040933.

Kurz, J. H., T. Jahr, and G. Jentzsch (2004), Earthquake swarm examples and a look at the generation mechanism of the Vogtland/Western Bohemia earthquake swarms, *Phys. Earth Planet. Inter.*, *142*, 75–88, doi:10.1016/j.pepi.2003.12.007.

Miller, S. A., C. Collettini, L. Chiaraluce, M. Cocco, M. Barchi, and B. J. P. Kaus (2004), Aftershocks driven by a high-pressure CO_2 source at depth, *Nature*, *427*, 724–727, doi:10.1038/nature02251.

Oliveira, R. G. (2008), Arcabouço geofísico, isostasia e causas do magmatismo cenozóico da Província Borborema e de sua margem continental, Nordeste do Brasil, Ph.D. thesis, Rio Grande do Norte Federal University, Natal, Brazil.

Poupinet, G., W. Ellsworth, and J. Frechet (1984), Monitoring velocity variations in the crust using earthquake doublets: An application to the Calaveras fault, California, *J. Geophys. Res.*, *89*(B7), 5719–5731, doi:10.1029/JB089iB07p05719.

Rowe, C., R. Aster, B. Borchers, and C. Young (2002), An automatic, adaptive algorithm for refining phase picks in large seismic data sets, *Bull. Seismol. Soc. Am.*, *92*(5), 1660–1674, doi:10.1785/0120010224.

Shipton, Z. K., A. M. Soden, J. D. Kirkpatrick, A. M. Bright, and R. J. Lunn (2006), How thick is a fault? Fault displacement-thickness scaling revisited, in *Earthquakes: Radiated Energy and the Physics of Faulting*, *Geophys. Monogr. Ser.*, vol. 170, pp. 193–198, AGU, Washington, D. C.

Simpson, D. W., W. S. Leith, and C. H. Scholz (1988), Two types of reservoir-induced seismicity, *Bull. Seismol. Soc. Am.*, *7*(6), 2025–2040.

Talwani, P., and S. Acree (1985), Pore pressure diffusion and the mechanism of reservoir-induced seismicity, *Pure Appl. Geophys.*, *122*, 947–965, doi:10.1007/BF00876395.

Talwani, P., L. Chen, and K. Gahalaut (2007), Seismogenic permeability, k_s, *J. Geophys. Res.*, *112*, B07309, doi:10.1029/2006JB004665.

Tomic, J., R. E. Abercrombie, and A. F. do Nascimento (2009), Source parameters and rupture velocity of small $M \leq 2.1$ reservoir induced earthquakes, *Geophys. J. Int.*, *179*, 1013–1023, doi:10.1111/j.1365-246X.2009.04233.x.

Wust-Bloch, G. H. (2010), Characterising and locating very weak ($-2.2 \geq ML \geq -3.4$) induced seismicity in unstable sandstone cliffs by nanoseismic monitoring, *Pure Appl. Geophys.*, *167*, 153–167.

Zhou, R., L. Huang, and J. Rutledge (2010), Microseismic event location for monitoring CO_2 injection using double-difference tomography, *The Leading Edge*, *29*(2), 208–214, doi:10.1190/1.3304826.

J. D. Kirkpatrick, Earth and Marine Sciences Department, University of California, Santa Cruz, CA 95064, USA.

R. J. Lunn and S. I. Pytharouli, Department of Civil Engineering, University of Strathclyde, Glasgow G4 ONG, UK. (stella.pytharouli@strath.ac.uk)

A. F. do Nascimento, Departamento de Geofisica, Universidade Federal do Rio Grande do Norte, Natal 59072-970, Brazil.

Z. K. Shipton, Department of Geographical and Earth Sciences, University of Glasgow, Glasgow G12 8QQ, UK.